Monitoring rebar corrosion propagation in concrete – Results of the Naxberg field experiment after 12 years

Yves SCHIEGG[1], Jan BISSCHOP[1], Stefanie VON GREVE-DIERFELD[1]

[1]Technology and Research for Concrete Structures (TFB AG), 5103 Wildegg, Switzerland
-schiegg@tfb.ch -

Abstract: This contribution reports the results of a 12-year long field experiment aimed at studying the corrosion behavior of ordinary and stainless steel rebars in various types of concretes. The test panel of 32 concrete plates is located in the wall of the Naxberg tunnel in Switzerland with a high supply of chlorides from deicing salts (exposure class XD3). All concrete plates have embedded sensors for in-situ monitoring the humidity (water uptake), temperature, chloride content of the concrete, and the corrosion initiation and progression of the reinforcement steel bars.

The plates generally showed a very strong ingress of chlorides over the 12 years as shown by the regular measurements of the chloride concentration profiles from cored samples. The chloride ingress rate was affected by the concrete type and the height distance from the road. The plates that were treated with a hydrophobic agent showed very little ingress of chlorides.

The non-destructive *in-situ* measurements of the corrosion currents (macrocell currents) showed that some rebars with a concrete cover of 10 mm already started corroding after one or two winters. For the concrete with a low w/c, depassivation of rebars at a depth of 20 mm was recorded after 2 to 4 years. After 12 years of exposure only the plates that contained stainless steel rebar or were hydrophobically treated showed no rust spots on the surface. By combining the in-situ measurement of corrosion initiation time and the measured chloride profiles, the critical chloride content (C_{crit}) for the various concrete types could be estimated.

Keywords: critical chloride content, corrosion initiation, corrosion propagation, stainless steel

Introduction

The design of durable concrete structures requires knowledge of the damaging mechanisms and the effect and effectiveness of various measures to counteract the damage. One of the main causes of damage to buildings of transport infrastructure is the rebar corrosion induced by the ingress of chlorides. Especially for transport infrastructure with deicing salts and spray water exposure, there is no consensus about which measures are most effective. The following contribution from the 12-year long Naxberg tunnel experiment shows the aspect of corrosion initiation and propagation for different reinforcement steel types and various concrete mixtures.

Field experiment panel in Naxberg tunnel

The Naxberg tunnel is located along the A2 motorway close to the Gotthard tunnel at around 1000 m altitude (asl). As a part of tunnel restoration work at the end of the 1990s, the opportunity was provided to place a concrete test in the tunnel wall at 50-meter distance from the north-facing tunnel entrance (Fig. 1). The panel consists of 32 concrete plates with dimensions of 600 x 500 x 100 mm. The plates were fixed to the wall with four anchor rods made of stainless steel (material no. 1.4529). All electrical connections of the sensors installed in the plates were fed into a measuring box next to the test plates. In this measuring box there are 4 data-loggers for continuous measurements and connections for manual measurements.

Due to the different position of the plates (height distance from road ≈ 0 to 2.4 m), the exposure class according to European standard EN 206 was expected to vary from XD3

(alternating wet/dry with exposure to chloride-containing spray water) to XD1 (moderately moist with exposure to chloride-containing mist water).

Fig. 1. *Visual state of test panels in Naxberg tunnel in year 2000 (left) and 2012 (right).*

Composition of concrete plates

The concrete plates were composed of 5 concrete types and 4 reinforcement types (see Table 1). A concrete with an average composition (w/c = 0.5 and 300 kg/m^3 CEM I 42.5) was taken as the reference concrete. In the plates indicated by D, E and F a part of the Portland cement was replaced by mineral additions (slag, fly ash, or silica fume). The G-plates differed from the reference concrete by a significantly lower w/c-value of 0.35. Plates A1 and A2 were hydrophobically treated in the laboratory after a given curing time.

Table 1. *Composition of investigated reinforced concrete types. The cover thickness varied between 10 and 40 mm.*

Nr.	Concrete type	Reinforcement type
H1-H4	w/c 0.5, CEM I (reference concrete)	carbon steel B500B
G1-G4	w/c 0.35, CEM I	
D1-D4	w/c 0.5, CEM I + 20% Slag (S)	
E1-E4	w/c 0.5, CEM I + 15% Fly ash (FA)	
F1-F4	w/c 0.5,CEM I + 7% Silica fume (SF)	
A1-A2	Reference concrete + Hydrophobic treatment	Top12, galvanized carbon steel, stainless-steels 1.4401, 1.4462
B1-B2	Reference concrete	Top12, galvanized carbon steel,
C1-C2	Reference concrete	stainless-steels 1.4401, 1.4462

In plates of series A, D to H, the reinforcement consists predominantly of ordinary, unalloyed B500B concrete steel. Plates B1, B2, C1, and C2 contained galvanized steel and differently alloyed, stainless-steel types (see Table 1): Top12 is a Cr-steel from Swiss Steel AG with a chromium content of more than 12%, The investigated stainless-steel types were 1.4401 (16.5% Cr, 10% Ni, 2% Mo) and 1.4462 (21% Cr, 4.5% Ni, 2.5% Mo, 0.1% N).

Instrumentation in the concrete plates

The lowermost concrete plates (numbered with '1') and plates H3, F3 and D3 were instrumented with chloride and resistance sensors for in-situ measurements as well as with reinforcement steel test bars (Fig. 2). The test bars (length ca. 10 cm) were electrically insulated and had varying cover thickness in range of 10-40 mm. The remaining concrete plates also contained the reinforcement test bars, but no further sensors. All concrete plates contained a “cathode” steel grid in the plate side facing the tunnel wall (see Fig. 2).

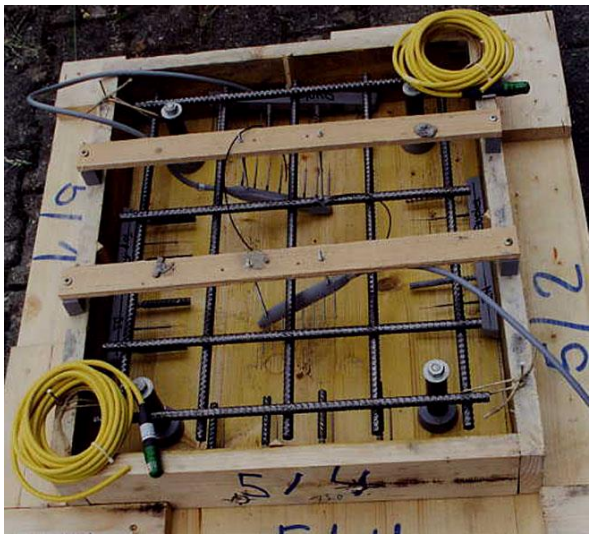

Fig. 2. *Instrumentation and reinforcement bars and grid embedded into the concrete plates (see text for explanation).The steel grid is positioned in the rear (wall) side of the plate.*

The following measurements were recorded with the sensors and insulated reinforcing bars:

- Potential and electrical resistance of concrete by means of the wire and rod sensors
- Macrocell currents (corrosion currents) between insulated reinforcing bars and the grid in the back side of the concrete plates
- Corrosion potential at the concrete plate surface
- Concrete temperature

Selected measurements were automatically recorded for plates D1 to H1 (measuring intervals of 10 minutes to 1 hour). Temperature and rel. humidity inside the tunnel were also recorded.

Sampling of rebars in 2012

After about 12 years, i.e., in the autumn of 2012, 7 plates were taken out of the test panel and transport to the laboratory. These were the plates H1 and H4 (reference concrete), G1 and G4 (w/c = 0.35), E3 (concrete with fly ash), and A1 (reference concrete with hydrophobic treatment). In order to obtain the reinforcement bars, the plates were carefully crushed in a compression setup (Fig. 3).

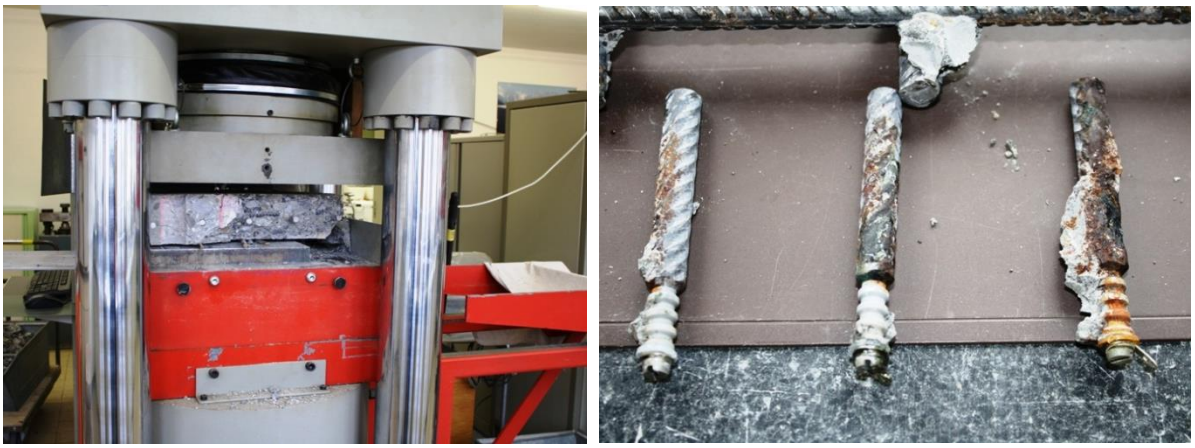

Fig. 3. *Left: Crushing of concrete plates to obtain the rebars. Right: corroded rebars obtained from test plates.*

Firstly, the visible corroded area of the steel bar surface was measured or estimated. Subsequently, the effective anode area and the depth of the steel removal due to corrosion was microscopically measured at Swiss federal laboratories for materials science and technology (EMPA). For this purpose, the rust on the bars was carefully removed.

The corroded areas were exactly traced in order to measure the size of these areas (Fig. 4). The corroded area was measured by means of image analysis (pixel counting). The mass loss by corrosion was estimated by a volume determination through underwater weighing.

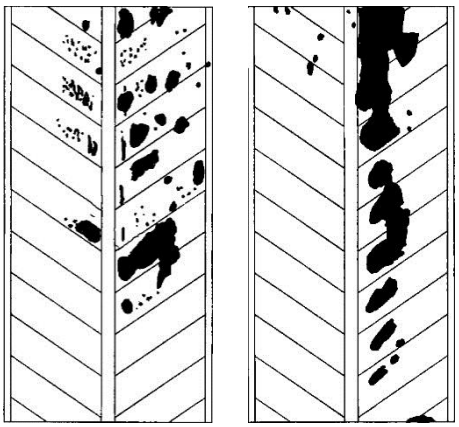

Fig. 4. *Example images of test bars showing the corroded area fractions in black.*

Results and discussion

Progress of carbonation

The carbonation depths were measured from the surface of drilled cores (Fig. 5). For the reference concrete (plates H1, H3 and H4 - w/c = 0.5), the carbonation depth increases significantly with height distance from road. The lower plates are most affected by spray water and snow accumulation, and therefore have a high water-saturated degree than the higher plates. The diffusion rate of CO_2 into saturated-concretes is typically lower that for partly saturated or dried concrete. In the case of concrete plate A1 (with hydrophobic treatment), the carbonation depth is significantly greater than in the case of plate H1. The higher carbonation depth is due to the water-repellent effect of the hydrophobic treatment which results in a higher diffusive CO_2-ingress. A comparatively high carbonation depth was measured for plate E3. It appears that the addition of fly ash resulted in a faster carbonation compared to the reference concrete. Approximate carbonation coefficients [1] for plates H1, H3 and H4 of, respectively, 0.7; 1.9; and 6.3 mm/year$^{0.4}$ were obtained from these measurements. The coefficient of the plate H4 is very high, which could be due to an increased CO_2 content of the air in the tunnel. For plate A1 a carbonation coefficient of 3.7 mm/year$^{0.4}$ was determined, which is between the values of the plates H3 and H4.

Chloride content in concrete plates

Chloride profiles were measured from cored samples at intervals (slices) of 10 or 15 mm. Some example profiles are depicted in Fig. 6. All chloride profiles measured in Naxberg experiment are published in [2]. For plate H1, the chloride content reaches about 0.5 w-% of cement at 30 mm depth after 2 winters, and this corresponds approximately to the critical chloride content for corrosion initiation. Three years later, the chloride content had markedly increased in terms of total quantity and depth. After 12 years, the concrete plate is severely

salted over its entire thickness (chloride content of 3 w-% of cement). The significantly lower chloride contents in the plate G1 show the effect of the lower w/c-value of 0.35 (density); the chloride profiles are generally also steeper with lower penetration front. Plate A1 with hydrophobic treatment shows very little chloride ingress throughout the exposure period of 12 years. There only is a small increase in chloride content in the immediate vicinity of both plate surfaces.

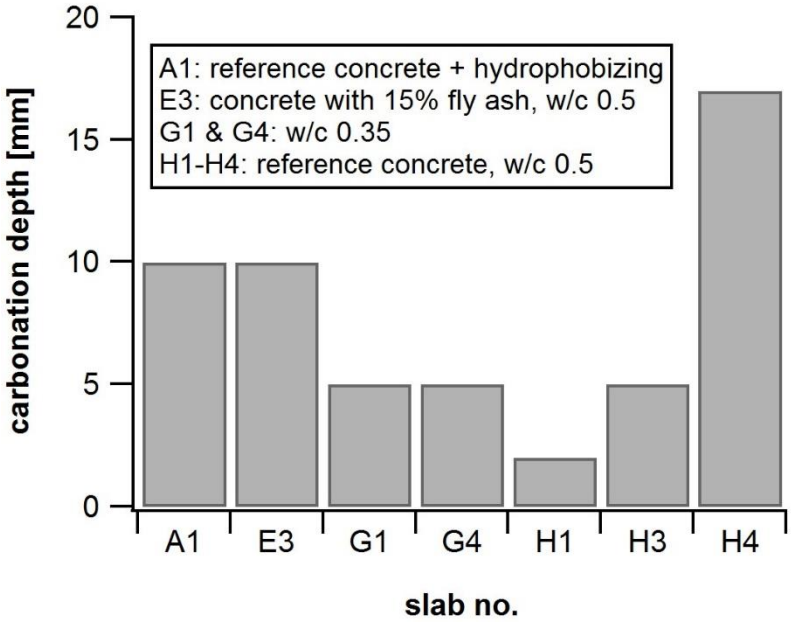

Fig. 5. *Carbonation depths measured in various concrete plates after 12 years exposure.*

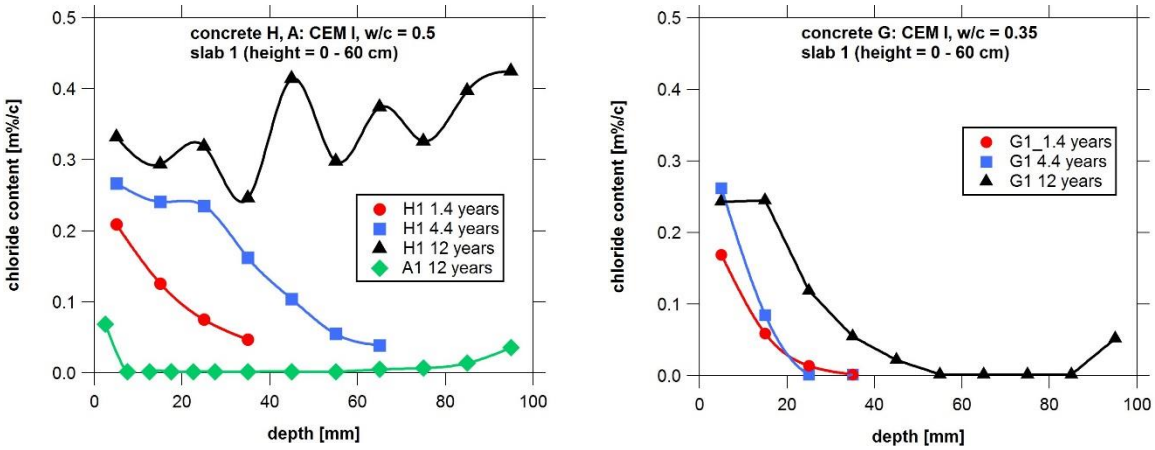

Fig. 6. *Chloride profiles in the lowest concrete plates H and G with CEM I.*

Initiation of corrosion and critical chloride content

The timing of corrosion initiation of the reinforcement could be reliably determined in most cases based on the measured macrocell currents (corrosion currents) and/or by the corrosion potential measurements. As long as the steel sensor is passive, i.e. free of corrosions, no or an extremely low current between the sensor and the rear reinforcement grid (cathode) is recorded. When the critical chloride content is exceeded, a local corrosion attack on the steel is triggered (initiation), which causes the current flow, i.e., macrocell current between the local separated anodes (corrosion site) and cathodes (Fig. 7). The stable initiation of pitting is, in most cases, a process that starts abruptly and leads to a rise in current. Short-term passivation and depassivation processes before the actual breakthrough, as can also be seen in

Fig 7, are typical for pitting corrosion induced by chlorides. After the initiation of the corrosion, a permanent current flow is registered, resulting in a gradual growth of the corrosion pits which is characterized as the corrosion progress.

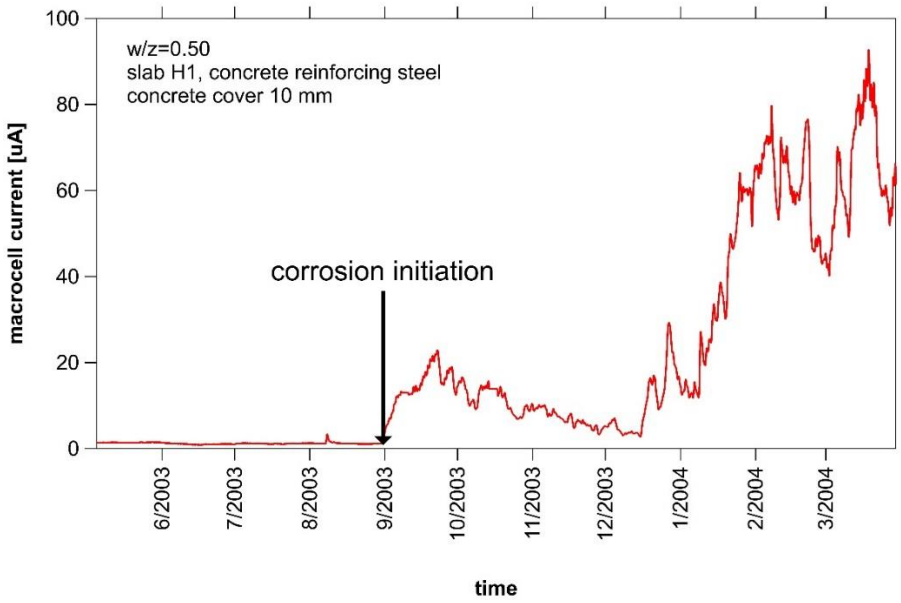

Fig. 7. *Evolution of the macrocell current for a B500B rebar in plate H1. From the moment of the corrosion initiation the current increases in a step-wise manner.*

The critical chloride contents (C_{crit}) determined during the field test in the Naxberg tunnel were in between 0.05 and 0.11 w-%/b for the carbon steel B500B (hot-rolled) and between 0.11 and 0.17 w-% of binder for the resistant steel type TOP12. For the stainless steel 1.4462, no critical chloride content could be determined, since the rebars remained corrosion-free up to the moment of sampling after 12 years of exposure. Table 2 shows the measured C_{crit}-values recalculated into a weight fraction of the actual Portland cement (CEM I) content. These results show that, apart from the dilution effect, there appears to be no large effect of mineral addition on C_{crit}. From the table, it can also be observed that C_{crit} for stainless steel 1.4462 must exceed the highest value in Table 2, namely 3.0 w-% of binder.

Table 2. *Average critical chloride content (C_{crit}) for carbon, TOP12, and stainless steel 1.4462 rebars.*

Concrete type	**C_{crit} (B500B)** [w-%/c]	**C_{crit} (Top12)** [w-%/c]	**C_{crit} (1.4462)** [w-%/c]
CEM I, w/c 0.5	0.40 – 0.80	1.39	> 2.46
CEM I, w/c 0.35	0.71	-	> 1.63
CEM I + 15% FA, w/b = 0.5	0.57	1.39	> 2.71
CEM I + 7% SF, w/b = 0.5	0.64	1.28	> 2.56
CEM I + 20% S, w/b 0.5	0.74	0.90	> 3.03
average	**0.64**	**1.24**	**> 2.48**

SF = Silica fume / FA = Fly ash / S = slag

Degree of rebar corrosion

Some examples of corroded or corrosion-free rebars (at cover depth of 10 mm) in the reference plate H3 are shown in Fig. 8. The carbon steel bars exhibit pitting and over 70% of the steel surface is corroded. This also applied to galvanized carbon steel bars. The zinc coating is virtually completely dissolved, and the underlying steel corroded with pitting. The resistant steel type TOP12 has only a few smaller rust spots without measurable material loss. The stainless- steel type 1.4462 is free of any corrosion signs.

Fig. 8*. State of corrosion of the rebars in concrete after 12 years chloride exposure and carbonation for plate H1 with cover thickness of 10 mm. From left to right: 2 x carbon steel B500B; 2 x TOP12; 2 x galvanized B500B; 2 x stainless steel 1.4462.*

After removal of rust from the rebar surfaces, the corroded area size and the maximum removal depth were measured using the abovementioned methods. The results of these investigations for the concrete steels with 10 mm cover thickness are shown in Fig. 9. In the case of plate H1 and H3, approximately 18% and, resp. 10% of the steel surfaces are attacked on average. It is striking that the carbon rebar in plate H4 is corroded 70% over its surface, although this plate is above the H1- and H3-plates. This is probably due to the larger carbonation depth, which leads to a combined or intensified corrosion attack together with the chloride ingress. Also in plate E3 (concrete with fly ash) the carbon steel rebars were relatively strongly attacked. The steel bars in plates A1, G1 and G4, on the other hand, had significantly smaller corroded surfaces and the corrosion pitting was less deep.

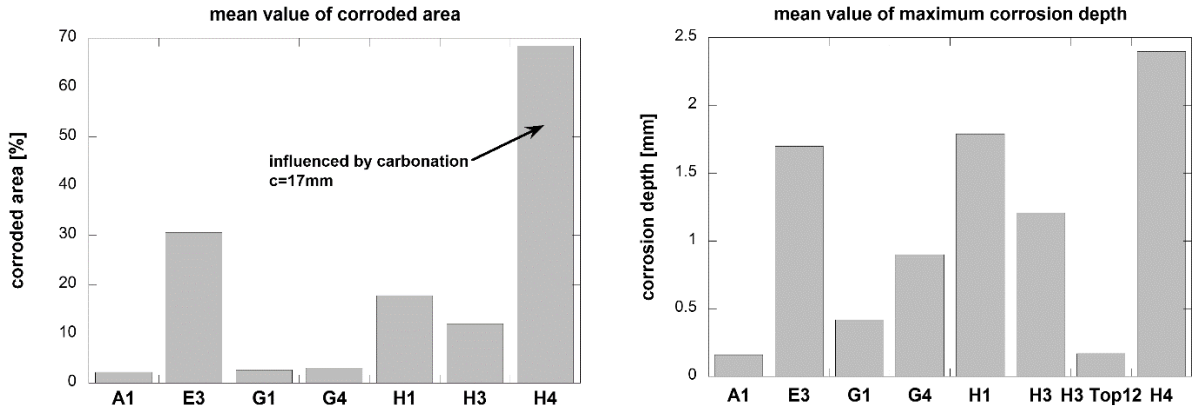

Fig. 9*. Average corroded surface fraction and average corrosion depth (max.) of rebars with cover thickness of 10 mm in plate H3.*

The average maximum corrosion depths correlate roughly with the corroded surface fraction (see Fig. 9). In the Plate A1 with hydrophobic treatment (and little chloride ingress), the carbon steel bars had relatively low corrosion degree (area and depth). The Top12-rebar in Plate H3 showed little corrosion depth as well.

Calculations of corrosion rate

On the steel samples, the macrocell current was measured between insulated reinforcing bars (anode) and the rear reinforcement grid (cathode) (see Fig. 2, 10). In order to make the data more easily understood, the current intensities were converted into current densities ($\mu A/cm^2$) or corrosion rates (mm/year) by using the corroded area measurements (= actual anode surface).

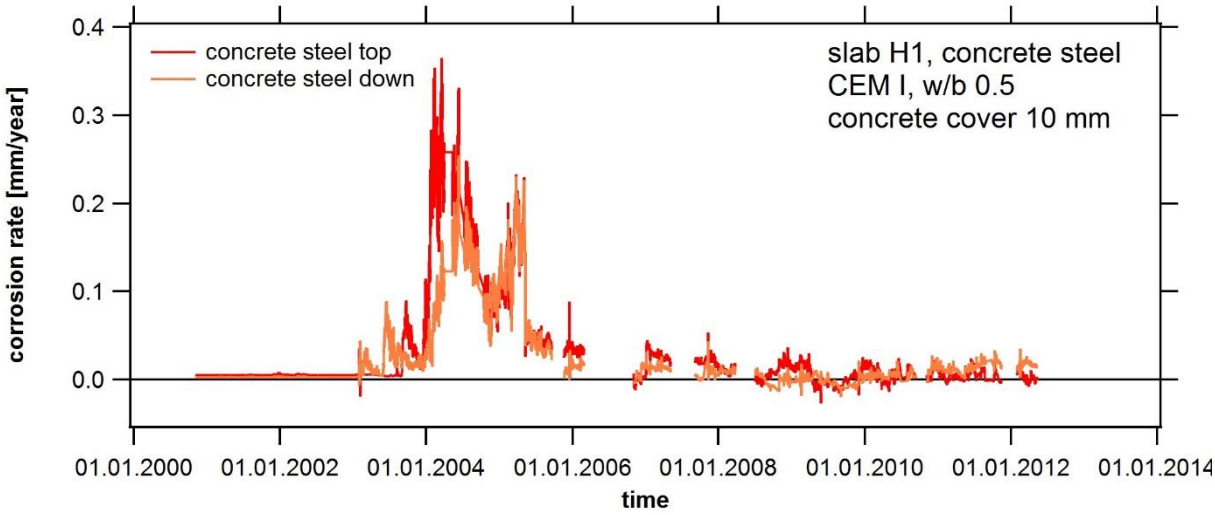

Fig. 10. *Corrosion rate for two carbon steel bars in plate H1.*

The corrosion rate increased sharply after initiation (after about two years into the field experiment). The short-term fluctuations in the corrosions rate (i.e., peaks) are likely a result of the temperature fluctuations of the concrete. In the summer months of 2004 and 2005 (warm temperatures), the corrosion rate is maximum, before it drops to below 0.1 mm/year and stabilizes for the next 6 years. Possible contributing cause of this drop in corrosion rate is the activation of the rear reinforcement grid, which reduces the passive cathodic performance of the grid reinforcement. The corrosion initiation of the deeper steel bars could also have led to a reduction in the corrosion rate of the top steel bars. The macrocell current can be converted into a mass loss over a certain time period by integrating the Faraday equation:

$$G = \frac{M}{z \cdot F} \cdot I \cdot t$$

G	*transferred mass*	*g*
M	*atomic mass*	*g/mol*
I	*current*	*A*
t	*time*	*s*
z	*valence*	*-*
F	*Faraday Constant*	*As/mol*

Fig. 11 shows the corrosion propagation (depth) of two carbon steel bars with a concrete cover of 10 mm in plate H4 (manual measurement). For the calculations, it was assumed that the measured corrosion area fraction represents the effective anode area size. For the ‘left’ carbon steel bar, the anode area was around 50% of the bar surface, whereas for the ‘right’ carbon steel bar this was 86%. The stepwise manner of the increase in corrosion depth is

probably related to temperature fluctuations. During the warm summer months, the corrosion rate is higher than in winter, because the electrical concrete resistance decreases with increasing temperature. Moreover, the moisture content of the concrete, accumulated in the winter, will be still high in (the beginning of) summer and facilitates corrosion. The average corrosion rate of the two reinforcing bars is comparable. For the 'right' carbon steel bar it is 0.019 mm/year (= 19 µm/year), whereas for the 'left' carbon steel bar the corrosion rate is slightly lower. The total steel removal calculated for these bars was about 0.15 mm after 9 years.

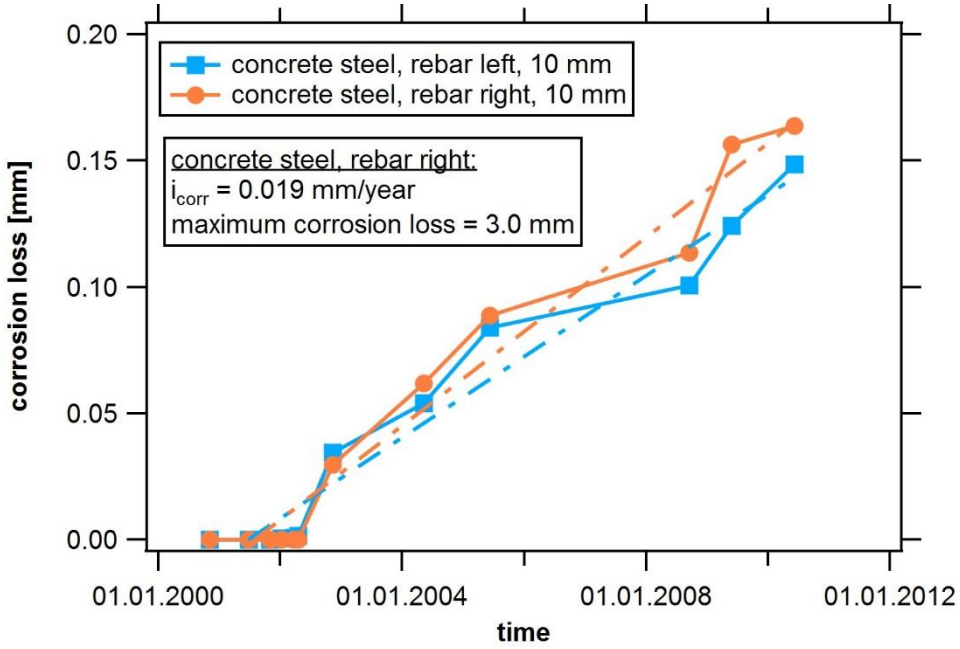

Fig. 11. *Progression of average corrosion depth for two carbon steel bars in plate H1.*

For the different concretes, the total steel removal amount at the moment of test bar sampling (in 2012) as gravimetrically measured, was up to two times higher than the calculated corrosion loss based on macrocell currents measurements. Several reasons for this difference are described in [3].

In practice, the anode area size as well as the corrosion depth increases with time. At the moment of initiation, the anode area is very small. With ongoing corrosion, the pits grow and expand into large cavities, and the corrosion depth increases as well. The assumption of a constant anode area size, on which the calculations in Fig. 11 are based, does therefore not correspond to reality.

In order to take the localization of the corrosion attack into account, a so-called pitting factor can be introduced to calculate the progress of corrosion more accurately. Recent investigations [4] have yielded pitting factors with values of between about 6 and 17. The pitting factor becomes smaller with time, because the anode area becomes larger as the corrosion progresses. Moreover, the increasing chloride content at the corrosion site also enhances the corrosion rate. Based on these considerations, it is to be expected that the corrosion rate rises markedly in the initial phase and stabilizes after a few years due to the increasing anodic resistance.

It is known from investigations in aqueous solutions that the corrosion rate reaches a maximum after some time and then decreases. This is explained by a hindering effect caused

by the precipitation of rather insoluble corrosion products [5]. The growth of the anode surface area can be considered by assuming that the growth is limited by diffusion-controlled rust growth processes according to following equation:

$$F_A = k \cdot \sqrt{t}$$

F_A = anode area size [mm²]

Fig. 12 shows the progress in the corrosion depths for two carbon steel bars in the plate H4 with assumed constant and √t-increasing anode area size. For the case of an increasing anode surface, the corrosion depth initially increases sharply and gradually stabilizes after about four years. The constant anode surface assumption leads to a more or less linear corrosion removal rate. By applying tangents to the growth curves, the maximum corrosion rate can be determined. For the 'left' rebar this is about 70 µm/year, which is a factor of 3.7 larger than the one determined for the linear growth assumption. For the 'right' rebar, the maximum corrosion rate was 260 µm/year. This is a factor of 10 times larger than in the linear case assumption for this sample. Corrosion rates in the range of 0.2 to 0.3 mm/year are plausible for comparable, heavily chloride-contaminated structures, as was also documented in earlier work [6].

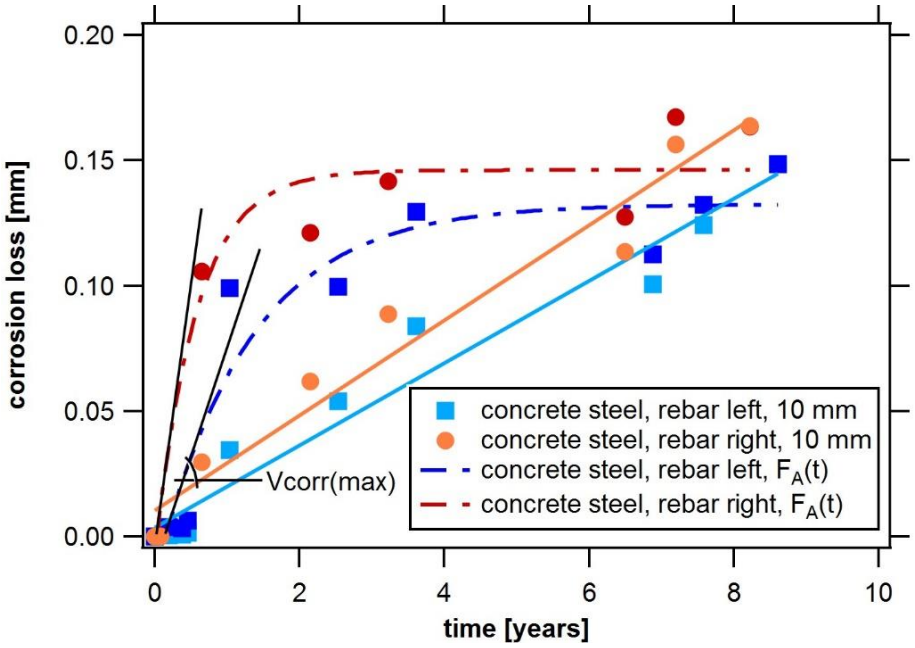

Fig. 12. *Progression of average corrosion depth for two carbon steel bars in plate H1 calculated on basis of assumed constant (conf. Fig. 11) or increasing anode area size F_A.*

Conclusions

With the instrumentation embedded in the concrete plates in the Naxberg tunnel, it was possible to detect the corrosion initiation moment of the reinforcement test bars and determine the corresponding critical chloride content (C_{crit}) by combining these *in-situ* data with the *ex-situ* measured chloride profiles. All plates with a w/c or w/b of 0.5 showed corrosion initiation within 8 years for carbon steel rebars with a concrete cover of 25-30 mm. Plates with hydrophobic treatment or a w/c of 0.35 showed no corrosion initiation under these conditions.

The rebar corrosion progress was monitored *in-situ* and *non-destructively* by measuring the macrocell currents between the corroding and non-corroding rebars in the concrete plates. The

total steel removal amount by corrosion calculated from the macrocell current intensities was about a factor two lower than the actual gravimetrically determined material loss after 10 years of corrosion. However, the initial corrosion rates of about 0.2 to 0.3 mm/year that followed from the *in-situ* macrocell current measurements are plausible values for vertical tunnel walls with high chloride loading under XD3 exposure.

References

1. F. Hunkeler, L. Lammar, Requirements for the carbonation resistance of concrete mixes, VSS report, no. 629 (2012)
2. J. Bisschop, Y. Schiegg, F. Hunkeler, Modelling the corrosion initiation of reinforced concrete exposed to deicing salts, VSS report no. 676 (2016)
3. Y. Schiegg, F. Hunkeler, H. Ungricht, D. Keller, Measures to increase durability – Sequel to the field study in the Naxberg tunnel, VSS report no. 683 (2017)
4. J. Harnisch, Investigations into the time dependent behaviour of electro-chemical and morphological parameters regarding the chloride induced corrosion of steel in concrete, Aachen, Technical University, Dissertation (2012)
5. F. Hunkeler, Basics of corrosion and potential mapping on concrete structures, VSS report no. 510 (1994)
6. Y. Schiegg, C.H. Voûte, H. Peter, S. Hasler, U. Urlau, Initiation corrosion propagation of stainless steel reinforcements in concrete structures. Nice, EUROCORR (2004)